Electrochemical and Solid-State Letters, **12** (2) A28-A32 (2009)
1099-0062/2008/12(2)/A28/5/$23.00 © The Electrochemical Society

Preparation of Nanotube TiO_2-Carbon Composite and Its Anode Performance in Lithium-Ion Batteries

Songhun Yoon,[a,z] Bok H. Ka,[b] Chulwee Lee,[a] Misun Park,[a] and Seung M. Oh[b,*]

[a]*Advanced Chemical Technology Division, Korea Research Institute of Chemical Technology (KRICT), Daejeon 305-600, Korea*
[b]*Research Center for Energy Conversion and Storage (RCECS), School of Chemical Engineering and Institute of Chemical Process, College of Engineering, Seoul National University, Seoul 151-744, Korea*

A nanocomposite between carbon and nanotube TiO_2 (CNTT) was prepared by addition of activated carbon during hydrothermal treatment of TiO_2 and following high-temperature calcinations. From morphological analysis using a scanning electron microscope, transmission electron microscope, and N_2 sorption profiles, it was revealed that nanotube TiO_2 was homogeneously dispersed with carbon in nanoscale for CNTT materials. When applied into the anode in a lithium-ion battery, CNTT electrodes displayed higher cyclability and better rate capability. From ac-impedance measurement, the total resistance was smaller in the CNTT electrode due to a homogeneously dispersed carbon in nanoscale and a more porous structure.
 [DOI: 10.1149/1.3035981]

Manuscript submitted September 22, 2008; revised manuscript received November 4, 2008. Published December 5, 2008.

Nanostructured titanium-oxide materials have attracted great interest as anode materials in lithium-ion batteries due to promising characteristics such as large capacity, high safety, and fast ionic transport in nanostructure.[1-6] TiO_2 has various kinds of phases such as TiO_2 (B), anatase, rutile, ramsdelite, and brookite.[2] When TiO_2 is nanostructured in nanowire or nanotube form, the diffusion path of Li^+ into the TiO_2 host becomes shorter, and resultantly fast charge/discharge characteristics appear.[1-5] During the formation of nanostructure, pore structure of TiO_2 should be optimized, because ionic transport within interparticle pores and volumetric capacity of electrodes are highly influenced by pore structures of nanostructured particles.[7] However, TiO_2 itself has intrinsically low electric conductivity of TiO_2 ($\sim 10^{-12}$ S cm^{-1}), which can be one of the shortcomings in the application of TiO_2 materials into the electrode of an electrochemical charge-storage device.[8] Although a conducting agent such as carbon black is added during electrode fabrication, further development of the conductive percolation network is desirable for the reduction of electronic resistance of the electrode. Along this line, Ag-modified TiO_2 nanotube was prepared by He et al.[9] In the practical point of view, however, cheaper and more available materials are recommended as electronic percolation enhancers. Furthermore, it has been reported that a high-crystalline TiO_2 phase appeared after high-temperature calcinations above 400°C. This well-developed crystalline structure resulted in a distinctive voltage plateau representing a more-ordered first-order phase transition from Li_xTiO_2 to $Li_{0.5}TiO_2$. This distinctive voltage plateau produced a cell-volume increase of 4%, and inevitable cycle fading appeared.[10] Hence, one can expect that cyclability of the TiO_2 anode will be improved if the crystalline structure is less developed even after calcination. For the preparation of nanotube anatase TiO_2, several authors reported that hydrothermal treatment of TiO_2 using high-alkaline conditions could produce nanotube TiO_2 at a low cost.[11]

In our study, a nanocomposite between carbon and nanotube TiO_2 is prepared by the addition of activated carbon during hydrothermal treatment of TiO_2. Nanosized TiO_2 is utilized as a precursor to prevent crystalline growth during high-temperature calcination. The conductivity enhancement by added carbon after hydrothermal treatment and concomitant pore structure change are investigated using the morphological analysis based on scanning electron microscopy (SEM), transmission electron microscopy (TEM), and N_2 sorption profiles. After fabrication of anode in lithium-ion batteries, cyclability, initial charge efficiency, and rate capability are analyzed and compared with nanotube TiO_2 prepared without carbon addition.

Experimental

Nanotube anatase TiO_2 was prepared under high-alkaline conditions.[3,11] Here, TiO_2 was provided by the Millennium Chemicals Company. TiO_2 used as a precursor was composed of 2–10 nm TiO_2 particles with 250 m^2 g^{-1} surface area, which was verified using a preliminary TEM experiment (see Fig. 1). To prepare nanocomposite between carbon and TiO_2, 3.5 g TiO_2 and 1.33 g activated carbon was added to 10 M NaOH 100 mL solution. The activated carbon was provided by the Ecopro Company. The surface area of the activated carbon was 750 m^2 g^{-1}. After 1 h stirring, the

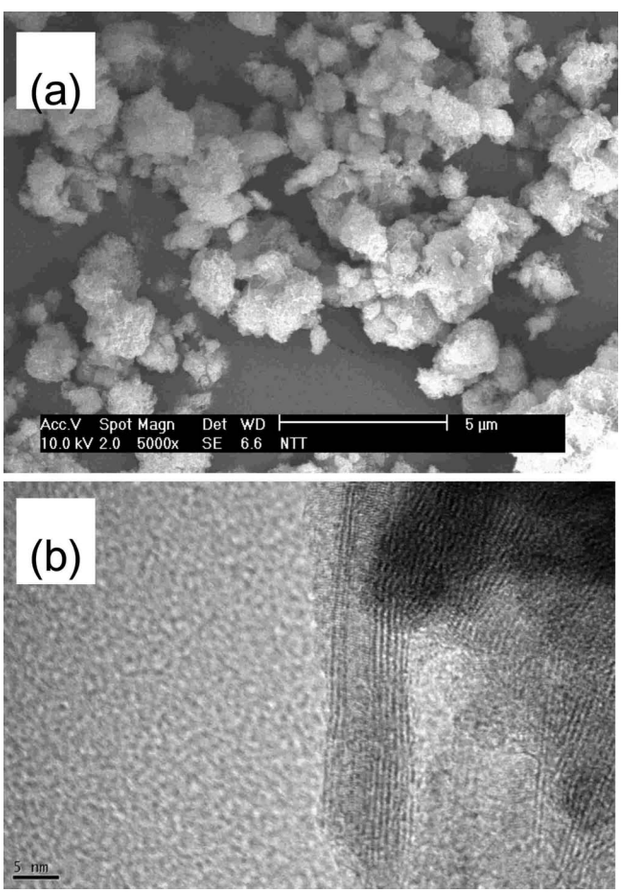

Figure 1. (a) SEM image and (b) TEM image of NTT.

* Electrochemical Society Active Member.
z E-mail: yoonshun@krict.re.kr

prepared slurry was reacted in an autoclave at 150°C for 72 h. After reaction within the autoclave, reacted slurry was added to 0.05 M HCl 500 mL solution. After stirring, the slurry was filtrated and washed. After drying at 80°C overnight, calcination was conducted at 400°C for 5 h.

Pore-size distribution was analyzed by N_2-adsorption measurement (Micromeritics ASAP 2010). External morphology of carbon was examined using SEM (JEOL JSM-840A), whereas the pore image was scanned by TEM (JEOL JEM-2010). X-ray diffraction (XRD) patterns were obtained with a Rigaku D/Max-3C diffractometer equipped with rotating anode and Cu Kα radiation (λ = 0.15418 nm).

To prepare the composite anodes, carbon powders were mixed with conducting agent (Super P) and polytetrafluoroethylene binder with a weight ratio of 8:1:1. The mixture was then dispersed in *n*-methyl pyrrolidone and spread on Ni foil (apparent areas 1 cm^2), followed by pressing and drying at 120 C for 12 h. The half-cell characteristics were analyzed in a coin-type (CR2016), two-electrode cell in which lithium foil (Cyprus Co.) was used. The electrolyte was 1.0 M $LiPF_6$ in ethylene carbonate (EC)/dimethyl carbonate (DMC) (1:1 volume ratio) (Tomiyama Co.).

To investigate anode performance in a lithium-ion battery, a coin cell was utilized, and galvanostatic charge–discharge in the voltage range from 2.5 to 1 V vs Li/Li^+ was conducted. The electrode loading was 15 mg cm^{-2}. The used electrolyte was 1.0 M $LiPF_6$ EC–DMC (1:1 v/v). For the rate-performance measurement, current was varied from 0.2C (30 mA/g) to 20C (3 A/g). The cycle performance for 70 cycles was recorded at 0.4C rate. All the electrochemical measurements were made with a WBCS-3000 battery cycler (Xeno Co.) at ambient temperature in a glove box filled with argon. For ac-impedance measurement, the frequency range was 10^6 Hz to 5 mHz with an ac amplitude of 10 mV (Zahner e6).

Results and Discussion

After hydrothermal treatment of raw TiO_2 using 10 M NaOH at 150°C, SEM and TEM images of prepared material were taken and are shown in Fig. 1. In the SEM image, homogeneously dispersed tubular morphology was observed, which was completely different from the original shape of raw TiO_2 composed of aggregated spherical particle (5–10 nm) shape. Clearly, tubular morphology was observed in the TEM image, as shown in Fig. 1b. This morphology was similar to that reported in the literature.[3,4,12] Hence, the prepared material is called nanotube titanium oxide (NTT).

Figure 2 shows SEM and TEM images of composite materials prepared by addition of activated carbon during hydrothermal treatment of TiO_2. The used activated carbon had irregularly shaped particles a few micrometers in size. As seen in Fig. 2a, however, any distinct morphological difference from NTT was not observed. Also, from the TEM image (Fig 2b), tubular-shaped morphology was predominantly observed, and an irregular part at the bottom also existed. From energy-dispersive spectroscopy analysis, 3.16 wt % (16.9 mol %) carbon was detected in the prepared materials. When compared with the initially added carbon amount (27.1 wt %) for hydrothermal reaction, a trace amount of carbon was found to remain. This was probably due to the oxidation of activated carbon at a high sintering temperature (400°C, 4 h). Though little carbon remained, its occupied volume was not negligible. Because of the low density of activated carbon (<1.5 gcc^{-1}) and the high density of TiO_2 (4 gcc^{-1}), carbon within the composite was calculated to occupy about 10 vol %, and the carbon phase was easy to detect in the TEM image. Hence, it is assumed that the irregular portion in Fig. 2b corresponds to the carbon phase and the other tubular part is TiO_2 phase. Consequently, a nanocomposite between carbon and tubular-shaped titanium oxide was produced and has been named carbon-nanotube titanium oxide (CNTT). Intrinsically, the low electric conductivity of TiO_2 ($\sim 10^{-12}$ S cm^{-1}) can be a shortcoming in the application of TiO_2 materials to the electrode of an electrochemical charge-storage device.[8] As CNTT homogeneously contained 3.16 wt % carbon in nanoscale, its electrical conductivity was expected to be much higher than NTT. This is discussed later in ac-impedance analysis.

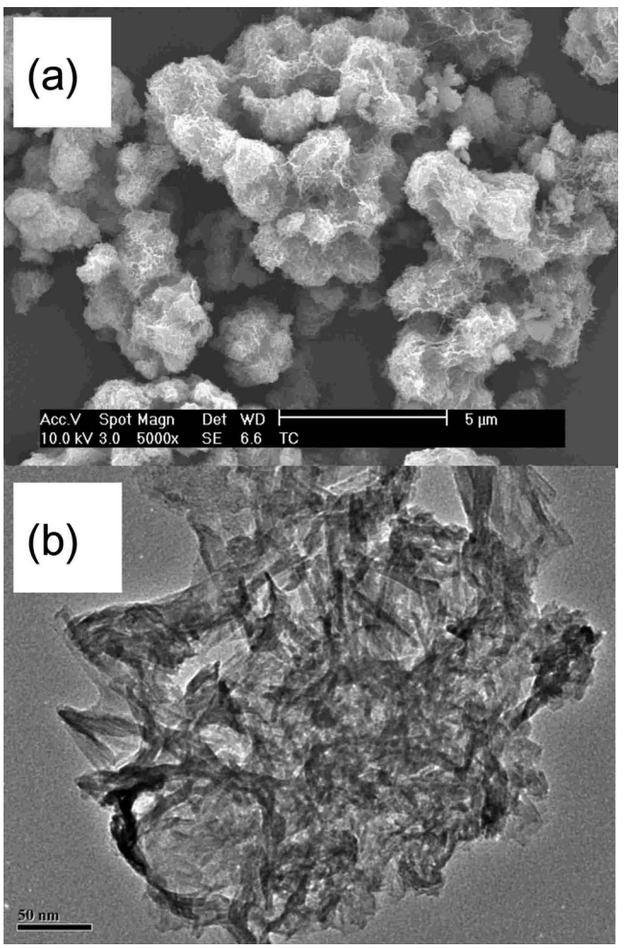

Figure 2. (a) SEM image and (b) TEM image of CNTT.

In Fig. 3, the Barrett–Joyner–Halenda (BJH) pore-size distribution of NTT (empty rectangle) and CNTT (empty circle) is displayed. The pores located near 10 nm were similar for both materi-

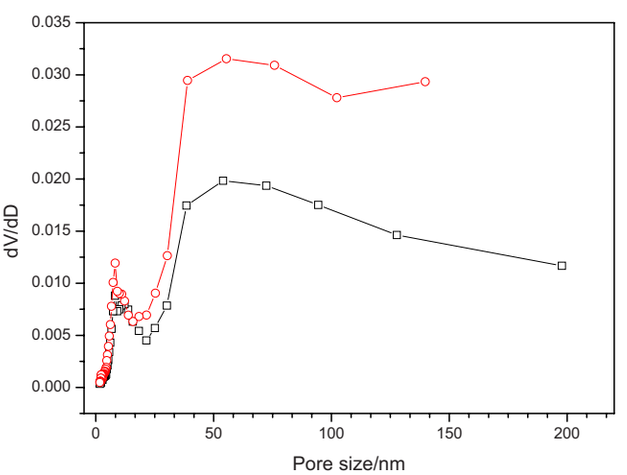

Figure 3. (Color online) Pore size distributions calculated by the BJH method in N_2-adsorption profiles measured with an ASAP 2010 instrument. Empty circle and empty rectangle are CNTT and NTT, respectively.

Table I. The comparison of physical properties and anode performance of NTT and CNTT.

Materials	A_{BET} (m^2 g^{-1})[a]	V_{pore} (ccg^{-1})[b]		C_{ch} (mAh g^{-1})[c]	C_{dis} (mAh g^{-1})[d]	IE (%)[e]	Cyc (%)[f]	Rate (%)[g]	R_{semi} (Ω g)[h]
		>30 nm	<30 nm						
NTT	78.5	0.11	0.12	165	137	83	85	32	0.079
CNTT	103.0	0.17	0.13	175	147	84	91	48	0.044

[a] BET surface area.
[b] Pore volume.
[c] Initial charging capacity.
[d] Initial discharging capacity.
[e] Initial efficiency (C_{dis}/C_{ch}).
[f] Capacity retention obtained discharge capacity at 70 cycles divided by C_{dis}.
[g] Rate capability at 20C.
[h] Sum of R_{SEI} and R_{ct} in Nyquist plot in Fig. 7.

als, but the population of pores above 30 nm was higher in CNTT. As shown in Fig. 2b, the mesopores generated among TiO_2 tube bundles were highly developed in CNTT. This coincided with the result in Fig. 3. Measured pore volumes above and below 30 nm are listed at Table I. Clearly, the difference in pore volume of the two materials lied above 30 nm. Furthermore, the Brunauer–Emmett–Teller (BET) surface areas of NTT and CNTT were 78.5 and 103 m^2 g^{-1}, respectively. Because of the high sintering temperature (400°C), the measured surface area of the two materials was relatively low when compared with nanotube prepared at a low sintering temperature.[3,12] Hence, although the reason is not clear, CNTT had a higher porous structure and larger surface area.

Figure 4 shows XRD results of NTT (Fig. 4a) and CNTT (Fig. 4b). NTT and CNTT display a similar crystallographic structure. According to the literature, measured XRD patterns contain anatase TiO_2 and $H_2Ti_2O_5{\cdot}H_2O$ structure.[3,4] Even after calcination at 400°C for 4 h, $H_2Ti_2O_5{\cdot}H_2O$ of monoclinic lattice was predominantly observed for both materials. Generally, one can expect that high specific surface energy induced by a large surface area facilitates crystal growth during calcination. Peak broadening in the XRD patterns of Fig. 4, however, indicate that the crystalline structure was less developed in NTT and CNTT, although the small-sized (5–10 nm) TiO_2 precursor was used for both materials. During hydrothermal treatment of precursor, heterogeneous species such as water and salt can be adsorbed in large amounts on the surface of nanosized particles. Hence, the retarded crystal growth in NTT and CNTT was probably attributable to these adsorptive species on the particle surface of TiO_2, which could impede the mass and ion transport during calcination. Peak indexes of $H_2Ti_2O_5{\cdot}H_2O$ and anatase TiO_2 are described with parentheses and brackets, respectively. From the peak-intensity comparison, $H_2Ti_2O_5{\cdot}H_2O$ phase was more dominant than anatase TiO_2. Interestingly, no peaks from carbon itself were detected in Fig. 4b, which was probably due to both the small amount of remaining carbon (3.16 wt %) and the amorphous crystalline structure of activated carbon.[13]

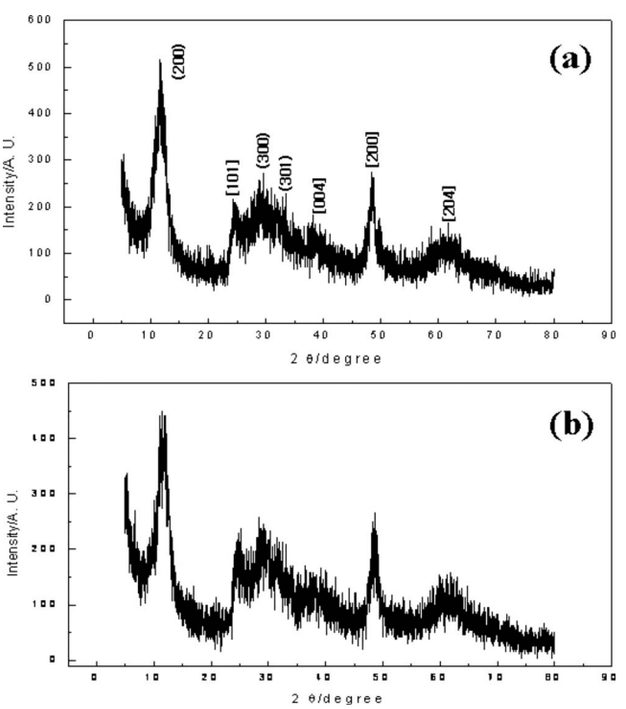

Figure 4. XRD pattern: (a) NTT and (b) CNTT. Peak indexes of $H_2Ti_2O_5{\cdot}H_2O$ and anatase TiO_2 are described with parentheses and brackets, respectively.

To investigate anode performance in lithium-ion batteries, electrodes were fabricated using prepared materials, and their anode performance was investigated. In Fig. 5, the galvanostatic charge–discharge profiles of NTT (Fig. 5a) and CNTT (Fig. 5b) during three cycles in the voltage range from 2.5 to 1 V vs Li/Li^+ are shown. The used current (rate) and electrode loading were 30 mA/g (0.2C) and 15 mg cm^{-2}, respectively. Clearly, one can observe that the CNTT electrode displayed a higher discharge capacity and a better initial charge efficiency than NTT. The reversible capacity of the CNNT electrode (147 mAh g^{-1}) was higher than the NTT electrode (137 mAh g^{-1}). This higher capacity was probably relevant to the higher electrical conductivity and well-developed porous structure of CNTT, indicating more efficient utilization of available charge-storage sites.

Although our materials were prepared at a high sintering temperature of 400°C for 4 h, the plateau located near 1.75 V was not distinct during charge/discharge. This plateau is known to be relevant to the distribution in composition caused by the preferential intercalation of small particles in TiO_2.[14] Furthermore, it was reported that the anatase TiO_2 phase became dominant after calcination above 400°C, accompanied by a clear voltage plateau during charge/discharge and an improvement of initial charge efficiency.[3] Consequently, the highly developed plateau represents a more-ordered first-order phase transition from Li_xTiO_2 to $Li_{0.5}TiO_2$, which resulted in the cell volume increase of 4%, and concomitant cycle fading was accelerated.[11] As seen in the XRD patterns of Fig. 4, however, the observed peaks of our materials were broad in comparison with the results reported by other researchers, reflecting that the TiO_2 crystal in our materials was not well developed.[5,12] From a practical point of view, a nondistinct plateau (smooth profile) is

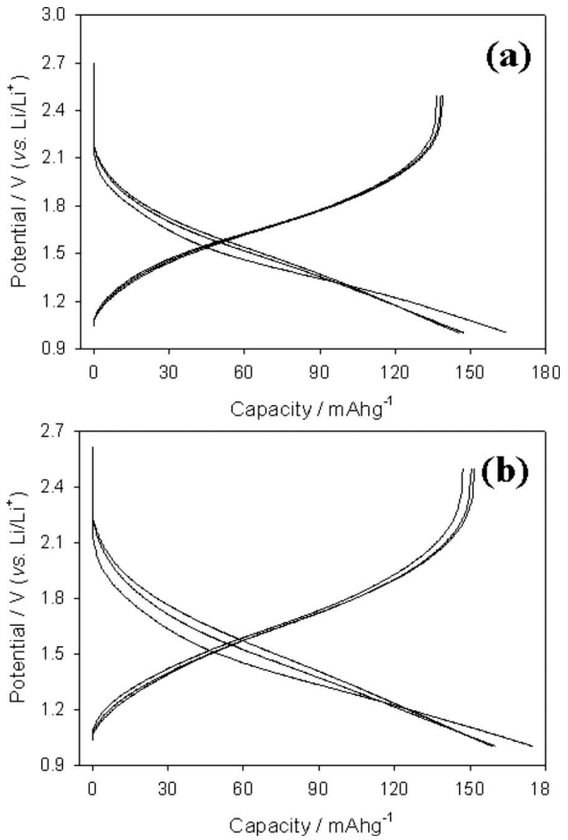

Figure 5. Galvanostatic charge–discharge profiles for three initial cycles in the potential range from 1 to 2.5 V vs Li/Li^+: (a) NTT and (b) CNTT. The electrolyte is 1.0 M $LiPF_6$ EC–DMC (1:1 v/v). The initial current (rate) and electrode loading were 30 mA/g (0.2C) and 15 mg cm^{-2}, respectively.

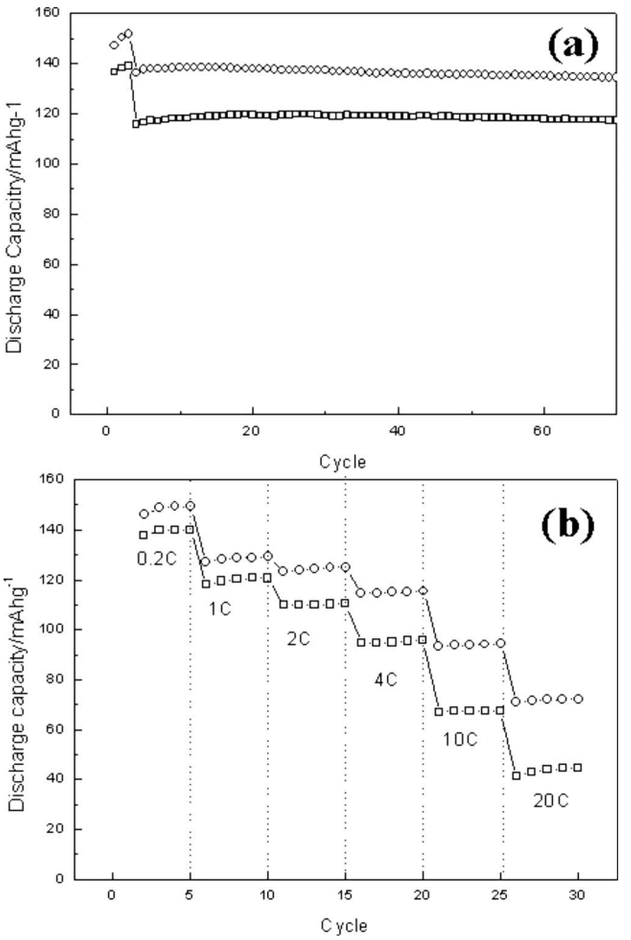

Figure 6. (a) Cyclability of NTT (empty rectangle) and CNTT (empty circle) for 70 cycles. In the initial three cycles, 30 mA/g (0.2C) was applied, and 0.4C current was used afterward. (b) Rate capability of NTT (empty rectangle) and CNTT (empty circle). Applied c-rate was described in the figure.

highly recommendable in large sized batteries used in hybrid electric vehicles (HEVs) and plug-in HEVs because of easy state of charge (SOC) prediction of lithium-ion cells.

The initial charge efficiency of Fig. 5 was as high as 83–84%, which is characteristic of TiO_2 materials sintered at higher temperatures above 400°C. Interestingly, in spite of the higher surface area, the CNTT electrode showed slightly higher initial charge efficiency. All of the physical and electrochemical properties are listed in Table I. Cycle and rate performance are illustrated in Fig. 6. CNTT electrodes displayed higher rate capability than NTT. The observed cycle performance was similar for both materials as shown in Fig. 6a, indicating the structural stability of nanostructured titania, which was related to a smooth voltage curve during charge–discharge (less strain induced by smaller volume change).[3,13] As shown in Fig. 6b, the rate capability of the CNTT electrode was superior to that of the NTT electrode. As listed in Table I, capacity retention of the CNTT electrode was as high as 68% at 10C (1.5 A/g) and 48% at 20C rate (3 A/g).

To elucidate the reason for improved rate performance of the CNTT electrode, ac-impedance analysis was conducted from 10^{-3} to 10^5 Hz frequency at 1.0 V vs Li/Li^+ after charging. The voltage of 1.0 V was selected, because the SOC was nearly half that of the fully charge state. In Fig. 7, ac-impedance spectra expressed as a Nyquist plot were illustrated. The characteristic shape for electrochemical faradaic reaction was observed.[9,15] The intercept at Z' axis is the bulk resistance (R_{elec}) of the electrolyte, separator, and electrode. Because cell geometry was identical in both electrodes, the smaller R_b in the CNTT electrode reflected the smaller electronic resistance of electrodes, which was due to carbon homogeneously

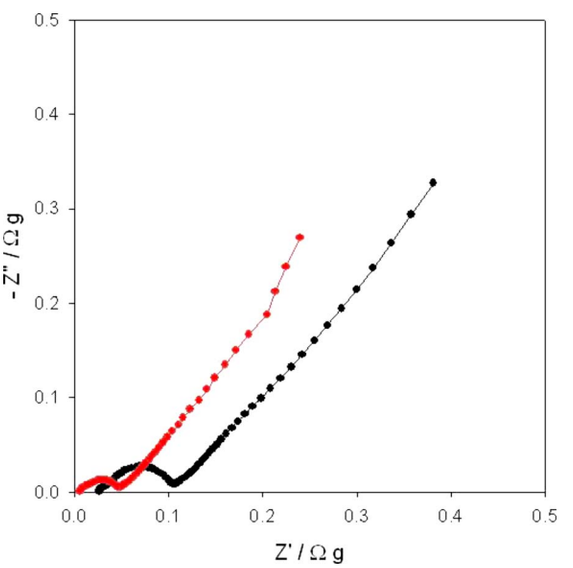

Figure 7. (Color online) The Nyquist plot from ac-impedance spectra for NTT (dark black) and CNTT (gray).

contained in CNTT (electronic percolation enhancer). Two partially overlapped semicircles appeared in the high-to-medium frequency region and a following straight sloping line was shown at the lower-frequency domain. The first two semicircles correspond to electrolyte transport resistance (R_{SEI}) in solid electrolyte interphase (SEI) and charge-transfer resistance of Li^+ (R_{ct}) into the TiO_2 particle.[9,15] The sum of R_{SEI} and R_{ct} is represented as R_{semi} in Table I, because it was difficult to separate them. Clearly, smaller R_{elec} and R_{semi} were observed in the CNTT electrode, indicating faster electrolyte transport within SEI and a higher charge-transfer rate of Li^+ in the CNTT electrode. This observed reduction of resistance in CNTT was probably due to a structural difference caused by homogeneously dispersed carbon in nanoscale, highly porous structure. This result is similar to phenomena observed when Ag was added to nanotube TiO_2.[9]

Conclusions

A CNTT was prepared by the addition of activated carbon during hydrothermal treatment of TiO_2. After calcinations, SEM and TEM images demonstrated that nanotube TiO_2 was homogeneously dispersed with 3.16 wt % (16.9 mol %) carbon in nanoscale. From pore size distribution, the population of pores above 30 nm was higher in CNTT, indicating that CNTT had a higher porous structure and larger surface area. When applied to the anode in a lithium-ion battery, CNTT electrodes displayed higher cyclability and better rate capability than NTT. The observed reversible capacity of the CNNT electrode (147 mAh g^{-1}) was higher than the NTT electrode (137 mAh g^{-1}). Also, capacity retention of the CNTT electrode was as high as 48% at 20C rate (3 A/g). From ac-impedance analysis, bulk resistance, SEI resistance, and charge transfer resistance were smaller in the CNTT electrode due to a homogeneously dispersed carbon in nanoscale, higher porous structure than NTT.

Acknowledgments

This research was supported by a grant from the Fundamental Research and Development Program for Core Technology of Materials funded by the Ministry of Knowledge Economy, Republic of Korea.

Korea Research Institute of Chemical Technology assisted in meeting the publication costs of this article.

References

1. A. R. Armstrong, G. Armstrong, J. Canates, and P. G. Bruce, *Angew. Chem., Int. Ed.*, **43**, 2286 (2004).
2. Y.-S. Hu, L. Keinte, Y.-G. Guo, and J. Maier, *Adv. Math.*, **18**, 1421 (2006).
3. J. Kim and J. Cho, *J. Electrochem. Soc.*, **154**, A542 (2007).
4. X. P. Gao, Y. Lan, H.-Y. Zhu, J. W. Liu, Y. P. Ge, F. Wu, and D. Y. Song, *Electrochem. Solid-State Lett.*, **8**, A26 (2005).
5. Z. Wang, S. Liu, G. Chen, and D. Xia, *Electrochem. Solid-State Lett.*, **10**, A77 (2007).
6. C. Jiang, I. Honma, T. Kudo, and H. Zhou, *Electrochem. Solid-State Lett.*, **10**, A127 (2007).
7. Z. Bing, Y. Yuan, Y. Wang, and Z.-W. Fu, *Electrochem. Solid-State Lett.*, **9**, A101 (2006).
8. I. Abayev, Z. Zaban, F. Fabregat-Santiago, and J. Bisquert, *Phys. Status Solidi A*, **196**, R4 (2003).
9. B.-L. He, B. Dong, and H.-L. Li, *Electrochem. Commun.*, **9**, 425 (2007).
10. R. V. Krol, A. Goosens, and E. A. Meulenkamp, *J. Electrochem. Soc.*, **146**, 3150 (1999).
11. T. Kasuga, M. Hiramatsu, A. Hoson, T. Sekino, and K. Nihara, *Langmuir*, **14**, 3160 (1998).
12. J. Li, Z. Tang, and Z. Zhang, *Electrochem. Solid-State Lett.*, **8**, A316 (2005).
13. J.-J. Lee, J.-K. Suh, J.-S. Hong, J.-M. Lee, Y.-S. Lee, and J.-W. Park, *Carbon*, **46**, 1648 (2008).
14. Q. Wang, Z. Wen, and J. Li, *Inorg. Chem.*, **45**, 6944 (2006).
15. S. Yoon, H. Kim, and S. M. Oh, *J. Power Sources*, **94**, 68 (2001).